13th International Conference on the Technology of Plasticity (ICTP 2020)

Title: Experimental and numerical investigations on the development and stability of residual stresses arising from hot forming processes

Author(s): Bernd-Arno Behrens[1], Jörg Schröder[2], Hendrik Wester[1], Dominik Brands[2], Sonja Uebing[2], Christoph Kock[1]

[1]Institut fuer Umformtechnik und Umformmaschinen
Leibniz Universität Hannover
An der Universität 2, 30823 Garbsen, Germany
E-mail: kock@ifum.uni-hannover.de

[2]Institute of Mechanics, Department of Civil Engineering
University Duisburg-Essen
Universitätsstraße 15, 45141 Essen, Germany

Abstract: Residual stresses are an important issue as they affect both the manufacturing process as well as the performance of the final parts. Taking the whole process chain of hot forming into account, the integrated heat treatment provided by a defined temperature profile during cooling of the parts offers a great potential for the targeted adjustment of the desired residual stress state. The aim of this work is the investigation of technological reproducibility and stability of residual stresses arising from the thermomechanical forming process. For this purpose, a long-term study of residual stresses on hot formed components is conducted. In order to develop finite element models for hot forming, a comprehensive thermomechanical material characterisation with special focus on phase transformation effects is performed. The numerical model is validated by means of a comparison between residual stress states determined with X-ray diffraction on experimentally processed components and predicted residual stresses from the simulations.

Keywords: forming process, finite element analysis, residual stress stability, X-ray diffraction

1. Introduction

In metal forming, the arising residual stresses influence the material behaviour during manufacturing as well as the performance of the final component [1]. In the past, the focus of forming process design was on minimising or eliminating residual stresses. However, residual stresses can also serve to improve the properties of the components through targeted use, for example with regard to distortions or wear behaviour [2]. This requires the residual stresses to be applied technologically in a reproducible manner and to remain stable over longer periods of time. In this context, reproducibility and stability of residual stresses particularly resulting from the four process types "peening and related surface treatments", "cold expansion of holes", "welding" and "machining" have been investigated by many authors, such as [3]. It is noticeable that most authors examine the development and stability of residual stresses in a strictly defined manner for a specific application. Depending on the type of process and the choice of material, which is linked to the process type, characteristic residual stress profiles are generated. For example, a typical feature of the surface treatment "shot peening" is a highly negative residual stress on the components surface, which decreases significantly towards the inside of the component [4]. Furthermore, it is known that relaxation and redistribution of residual stresses occur due to static or dynamic mechanical loads and thermal exposure. Static relaxation of residual stresses was for example investigated by [5] and [6] on components treated by shot peening. It should be noted that relaxation and redistribution of the local residual stresses occur when the accumulated residual stresses and the applied stresses due to subsequent mechanical loading exceed the yield state of the material. An important issue for many mechanical components is the potential effect of cyclic mechanical loads on the relaxation and redistribution of residual stress, even if the individual mechanical load cycles do not cause macroscopic plastic deformation. For example [5] and [7] investigated the stability of the peening residual stresses. It turned out that the residual stress relaxation is more significant for larger cyclic stress or strain. Little or no relaxation of peening residual stresses occurs, especially for small fatigue stress amplitudes [8]. Furthermore, e.g. in [9], the hole expansion process has shown that thermal exposure also leads to stress relaxation. In this case, the stress relaxation in aluminium samples was investigated at temperatures around 100 °C.

After 250 h of thermal exposure they noticed a low relaxation (5 to 15 %) and relatively small changes in fatigue life.

Until now, little attention has been paid to the stability as well as the calculation of residual stresses resulting from hot forming processes. The cost-efficient virtual process design of individual process steps or even an entire process chain is gaining in importance due to economic globalisation, continuously rising energy costs and growing competition in the manufacturing industry. Especially in the field of hot forming, process design in trial and error approaches represents a substantial cost and time expenditure [10]. At the same time, hot forming offers great potential for energy-efficient production of components by integrated heat treatment in the cooling phase after forming. Due to the numerous process parameters during forming, such as forming speed, plastic strains etc. as well as the temperature profile in the subsequent cooling process, there are numerous control parameters influencing the residual stresses. Nevertheless, the finite element (FE) simulation-supported design of hot forming processes using polymorphic steels is very challenging. As shown in Figure 1a, numerous influencing parameters from thermal, metallurgical and mechanical fields exist, which affect each other in complex interactions [11, 12]. For realistic process simulation, an appropriate mathematical model capable of consistently describing the polymorphic material behaviour is required. For this purpose, fully coupled thermo-mechanical-metallurgical FE simulations based on the theory of additive strain decomposition method are often used in literature [13, 14]. The resulting strain components are structured in Figure 1b according to their physical origin.

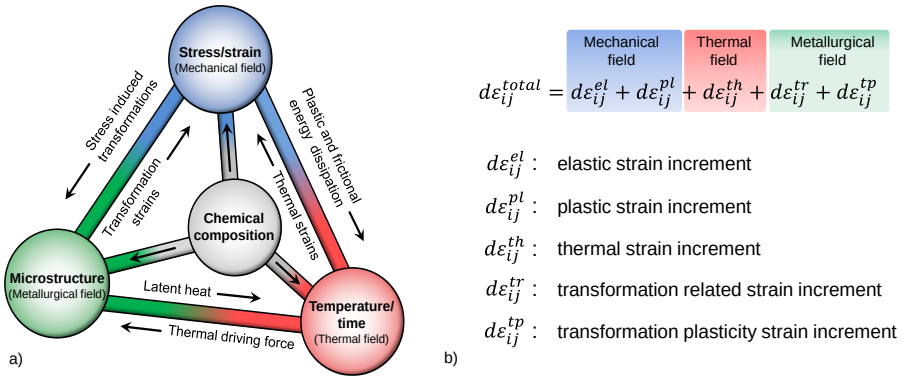

Figure 1: Interrelated thermo-mechanical-metallurgical material phenomena during thermo-mechanical processing of steel [6] (a) and basic principles of the additive strain decomposition method (b) [15].

This article presents the material modelling of two typical hot forming steels with the aim of calculating the residual stresses arising from the thermomechanical process. An experimental hot forming process is carried out and the resulting residual stresses are investigated in a long-term study with respect to their stability. Furthermore, an FE model is created and validated on the basis of the comprehensive experimental data. The FE-model validated in this work is intended to serve in future work as a virtual tool, enabling the determination of process parameters for inducing favourable residual stresses in hot-formed components. As an example, with the help of FE based process design residual compressive stresses should be generated in components such as crankshafts or gears to increase the product lifetime.

2. Material characterisation of hot forming steels

For the investigations in this work, the typical hot forming steels with the material numbers 1.3505 (AISI 52100) and 1.7225 (AISI 4140) according to German standards were used. The chemical composition of the two materials are listed in Table 1.

Table 1: Chemical composition of steel alloys 1.7225 and 1.3505 according to international standards [16] and [17].

[wt%]	C	Si	Mn	P	S	Cr	Mo	Fe
1.3505	0.99	0.25	0.35	0.025	0.015	1.475	0.10	balance
1.7225	0.42	0.25	0.75	0.025	0.035	1.10	0.22	balance

As outlined in the introduction, a comprehensive material characterisation is required to model the numerous thermal, metallurgical and mechanical material phenomena arising from the thermomechanical process. To simulate the plastic deformation behaviour during hot forming, compression tests were performed on the Gleeble

3800-GTC physical forming simulator with cylindrical samples of 10 mm diameter and 15 mm length. The flow curves were determined in the relevant temperature range (T=900, 1000, 1100 and 1200 °C). In addition, the tests were carried out at the corresponding temperatures with the equivalent plastic strain rates of $\dot{\varepsilon}_{eq}$ = 10 s^{-1} and 50 s^{-1}. Figure 2 shows the experimentally determined flow curves exemplarily for material 1.3505 at different temperatures and the strain rate $\dot{\varepsilon}_{eq}$ = 1 s^{-1} as well as for T = 1000 °C and different strain rates. A strict temperature and strain rate dependence of the strain hardening behaviour could be observed for both materials.

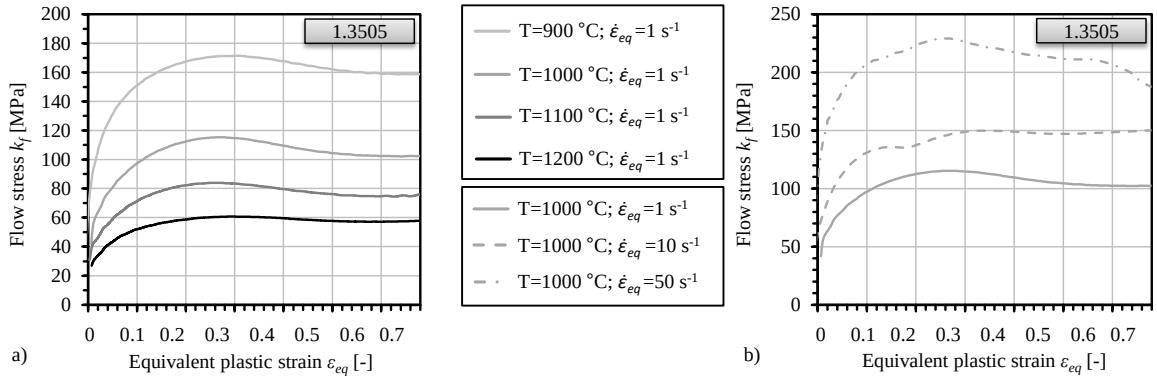

Figure 2: Flow curves of 1.3505 for different temperatures *T* (a) and different strain rates $\dot{\varepsilon}_{eq}$ (b) determined in upsetting tests at the Gleeble 3800-GTC [18].

In order to ensure a continuous description of the flow behaviour for the process simulation as a function of the equivalent plastic strain, the equivalent plastic strain rate and the temperature, the analytical approach of the so-called GMT model [19] for calculating the yield stress was calibrated. Equation 2-1 shows the calculation approach whereas the determined coefficients c_1, c_2, n_1, n_2, l_1, l_2, m_1 and m_2 of the analytical approach for both materials are listed in Table 2.

$$k_f = c_1 e^{c_2 T} \varphi^{n_1 T + n_2} e^{\frac{l_1 T + l_2}{\varphi}} \dot{\varphi}^{m_1 T + m_2} \qquad \textbf{(2-1)}$$

Table 2: Fitted GMT model parameters for 1.3505 and 1.7225.

Material	c_1 [MPa s]	c_2 [°C^{-1}]	n_1 [°C^{-1}]	n_2 [-]	l_1 [°C^{-1}]	l_2 [-]	m_1 [°C^{-1}]	m_2 [-]
1.3505	3113.02	-0.0033	5.0507*10^{-5}	-0.1090	-2.0135*10^{-5}	0.0024	6.6491*10^{-4}	-0.5000
1.7225	6054.21	-0.0039	-3.0846*10^{-5}	0.3000	1.8926*10^{-5}	-0.03548	-9.4422*10^{-5}	0.2484

In order to model the phase transformation behaviour during cooling after the forming process, continuous cooling transformation diagrams (cct diagrams) have been determined in experimental studies. Thereby, the phase transformation behaviour was investigated both without and with a previous deformation of the fully austenitised material. These diagrams are shown in Figure 3.

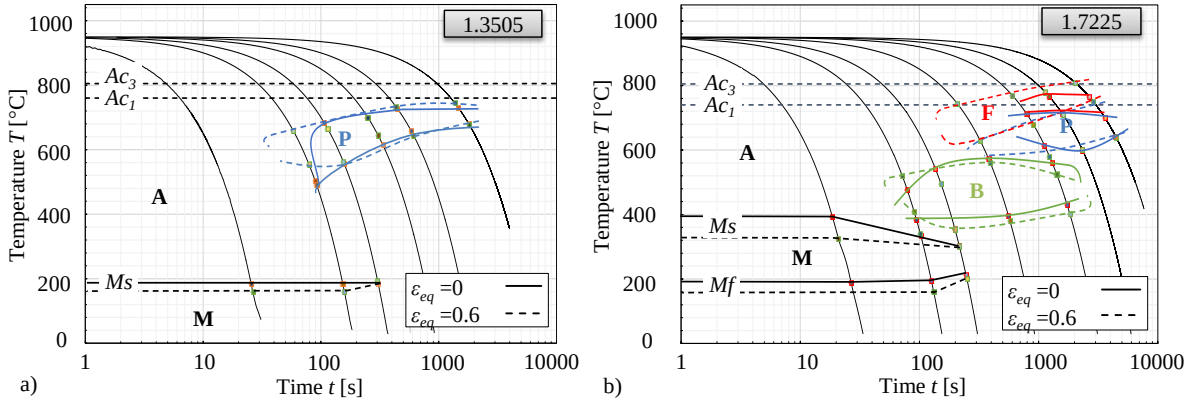

Figure 3: Continuous cooling transformation diagrams for the materials 1.3505 (a) and 1.7225 (b) [20].

It can be clearly seen that a previous deformation influences the microstructural transformation behaviour of both materials investigated significantly. For example, a reduction in the martensite start temperature Ms was found in each case. From these cct diagrams, time temperature transformation diagrams (ttt diagrams) were determined and

implemented in the Simufact.forming software. Further information on the investigation of phase transformation has already been published in [20] by the authors.
Besides the strains due to phase transformation, the transformation plastic strains (TRIP strains) were investigated by the authors in [21]. For this purpose, the phase transformation behaviour of the materials at a superimposed stress was investigated. The phase-specific TRIP coefficients listed in Table 3, were determined as characteristic material parameters.

Table 3: The phase specific coefficients of transformation plasticity for 1.3505 and 1.7225 [21].

1.7225		1.3505	
Phase	TRIP coefficient K_n [MPa^{-1}]	Phase	TRIP coefficient K_n [MPa^{-1}]
Martensite	$1.54*10^{-4}$	Martensite	$4.85*10^{-5}$
Bainite	$1.01*10^{-4}$	Pearlite	$6.17*10^{-5}$

In addition to the austenite flow curves, the ttt diagrams and the transformation plasticity coefficients, further phase-specific data are required for the correct modelling of the thermomechanical forming process. This comprises, for instance, characteristic data on specific heat capacity, latent heat or phase specific flow curves. In most cases, it is difficult to generate experimental material data for pure microstructural phases [22]. For this reason, supplementary material data have been generated with the thermodynamic simulation software JMatPro [23]. With the help of this software, it is possible to generate mechanical and thermal material data by means of thermo dynamic calculation approaches from [24] and [25] based on the chemical composition of the steel alloys. Further details on the material data used for simulation of the hot forming process can be found in [18].

3. Experimental and numerical procedure for thermomechanical processing of cylindrical specimen with eccentric holes

An experimental reference process was carried out to investigate the residual stress development in hot forming and to validate the material models created. The specimens were provided with thermocouples for a temperature-controlled process management. Subsequently, as shown in Figure 4a, the specimens were placed in a thermobox to ensure a quasi-isothermal test procedure during the forming phase. Within the thermobox the specimens were heated up to 1000 °C in a furnace. A ten-minute holding time was applied to ensure complete austenitisation. Afterwards, the thermobox with the specimen was transferred from the furnace to the servo hydraulic forming simulator VHS8800 (Instron GmbH). The specimens were upset at a punch speed of 200 mm/s to a final height of 28 mm from the initial height of 50 mm. The untreated specimen is shown schematically in Figure 5a whereas the deformed specimen is shown in Figure 5b in the cross-sectional view. Immediately after the forming process, the specimen was removed from the thermobox and cooled down to room temperature either in ambient air or in water. Due to the different cooling routes, different phase transformation phenomena are expected in the material, which lead to different residual stress profiles. In these tests cylindrical specimens with eccentric holes as shown in Figure 4b were used. Due to the asymmetrical hole, an inhomogeneous development of the residual stresses is expected in the material. For a statistical verification of the residual stress measurements, five identical tests were performed for each cooling medium and material. The experimental test procedure is described in detail in [18].

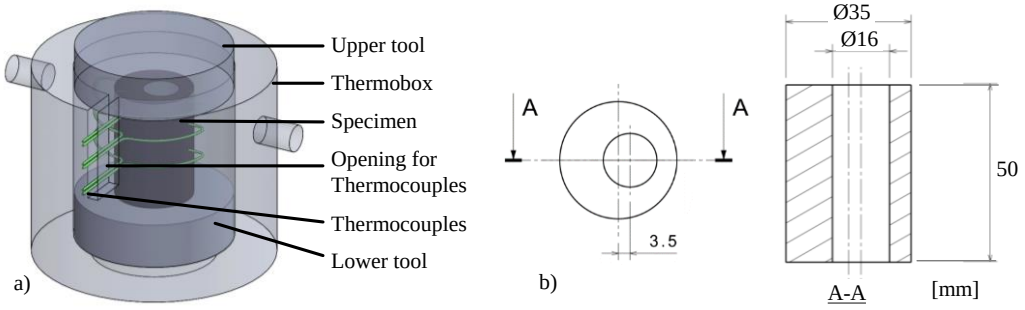

Figure 4: Schematic representation of the specimen prepared with thermocouples in a thermobox (a) and shape of the investigated specimen with dimensions in mm (b).

X-ray diffraction is used for residual stress analysis. The respective measuring point was initially polished electrolytically in order to avoid influences on the analyses from the scale layer of scale arising in the hot forming process. Subsequently, the tangential residual stresses were determined with the X-ray diffractometer X3000G2 (Stresstech GmbH) employing Cr-Kα radiation according to the corresponding DIN standard [26]. The measuring point was defined by a collimator with a diameter of 2 mm. Nine tilting positions of the measuring device were used per measuring point for stress evaluation. Afterwards, the measurements were evaluated with the software XTronic (Stresstech GmbH) by means of the sin² method. The values for the X-ray elasticity constant $½s_2 = 5.81*10^{-6}$ mm²N⁻¹ and the reference values for the unstressed material (d_{211} = 1.1703 Å, $2\theta_{Cr}$ = 156.084 °) were taken from the tabular data collection of [27]. These data of X-ray elasticity constants were calculated as mean values from the so-called Voigt [28] and Reuß [29] approaches for the pure alpha iron lattice.
The measuring points were placed at the mid-height of the specimen (cf. Figure 5b). Comprehensive residual stress measurements were carried out the following days after the thermomechanical treatment. The tangential residual stresses on the surfaces of the specimen were determined as shown in Figure 5b on the thick-walled side, measuring point 1 (MP1) and on the thin-walled side (MP2) of the specimen. In addition, further measurements along the circumference of the specimen were taken at angles θ = 45 °, 90 °, 135 ° according to Figure 5c. The X-ray measurement was additionally repeated several times per measuring point, to minimise the instrumental error, adjustment of the measurement system and effect of specimen curvature on the results. The investigation of the specimen, which has undergone the same experimental procedure each, is intended to make a statement about the technological reproducibility of the residual stresses. Additionally, subsequent to the immediate X-ray measurements, the measurements on MP1 and MP2 were repeated after six months and twelve months. In the meantime, the specimens were stored in a laboratory cabinet at a constant temperature of 20 °C. Thus, a statement on the stability of the residual stresses generated by the thermomechanical treatment can be made.

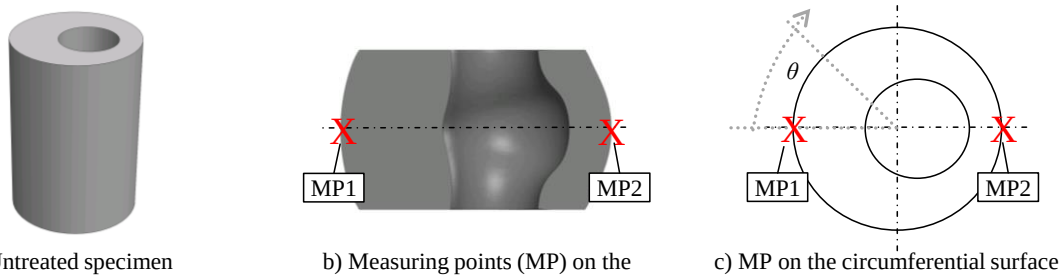

a) Untreated specimen

b) Measuring points (MP) on the mid-height of the specimen

c) MP on the circumferential surface indicated by the angle θ

Figure 5: Illustration of the untreated specimen (a), the measuring points MP1 and MP2 at the mid height of the specimen, (b) as well as the angle θ on the circumference of the specimen.

The experimental reference process described above was modelled with the commercial FE software Simufact.forming based on MSC.Marc solver. For this purpose, the comprehensive material data presented in section 2 were implemented in the software. In the simulation the heating process was modelled by a volume expansion of the specimen due to the austenitic phase transformation as well as the thermal expansion of the material.
At the beginning of the forming process a stress-free state in the specimen consisting of 100 % austenitic sample is assumed. A schematic representation of the FE model and the boundary conditions are shown in Figure 6.

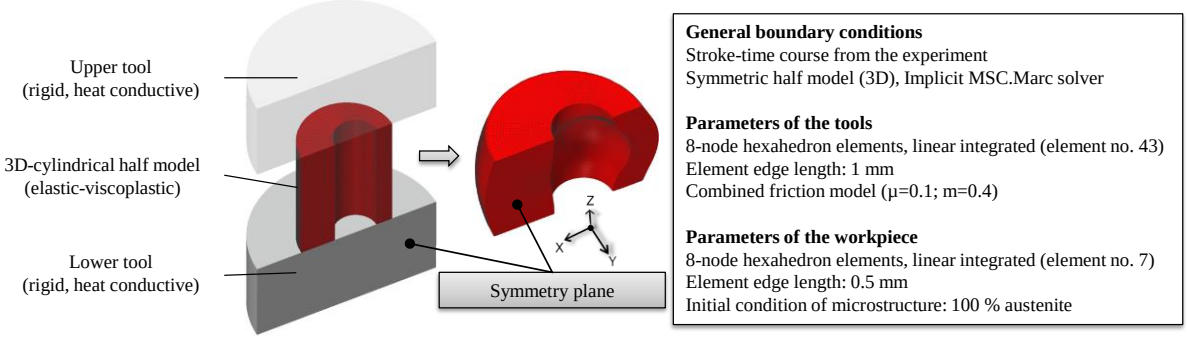

Figure 6: Design of the investigated FE simulation model with the boundary conditions.

The tools are considered as heat conducting rigid bodies and provided with a mesh of 1 mm element edge length. For the tools of the material 2.4668 (AISI: Inconel-718) constant values of the specific heat capacity c_p = 435 $Jkg^{-1}K^{-1}$ and heat conductivity λ = 11.4 $Wm^{-1}K^{-1}$ were taken from the data of the supplier [30]. The workpiece is assigned with an adaptive hexagonal mesh with the minimum element edge length of 0.5 mm, determined in a mesh sensitivity analysis.

4. Results of long-term X-ray analysis and FE model validation

The tangential residual stresses calculated in the simulations and the results of the experimental long-term X-ray analyses are shown in Figure 7. Considering the results of the residual stress measurements immediately after the hot forming tests, it is noticeable that the residual stresses due to rapid cooling in water are higher than those after cooling in air. After cooling in water, for the material 1.3505 residual stresses of σ_t = 216 MPa at MP1 and σ_t = 138 MPa at MP2 are determined, for the material 1.7225 σ_t = 212 MPa at MP1 and σ_t = 192 MPa at MP2. After cooling in air, however, significantly lower stresses of σ_t = -83 MPa at MP1, σ_t = -52 MPa at MP2 for 1.3505 and σ_t = 27 MPa at MP1, σ_t = 19 MPa at MP2 for 1.7225 are measured. At high cooling rates, a diffusion-free transformation of the austenitic into the martensitic phase takes place in the material, which leads to severe stresses in the crystal lattice. During diffusion-controlled phase transformation, which occurs while cooling in air, comparatively lower residual stresses in the range of zero can be observed.

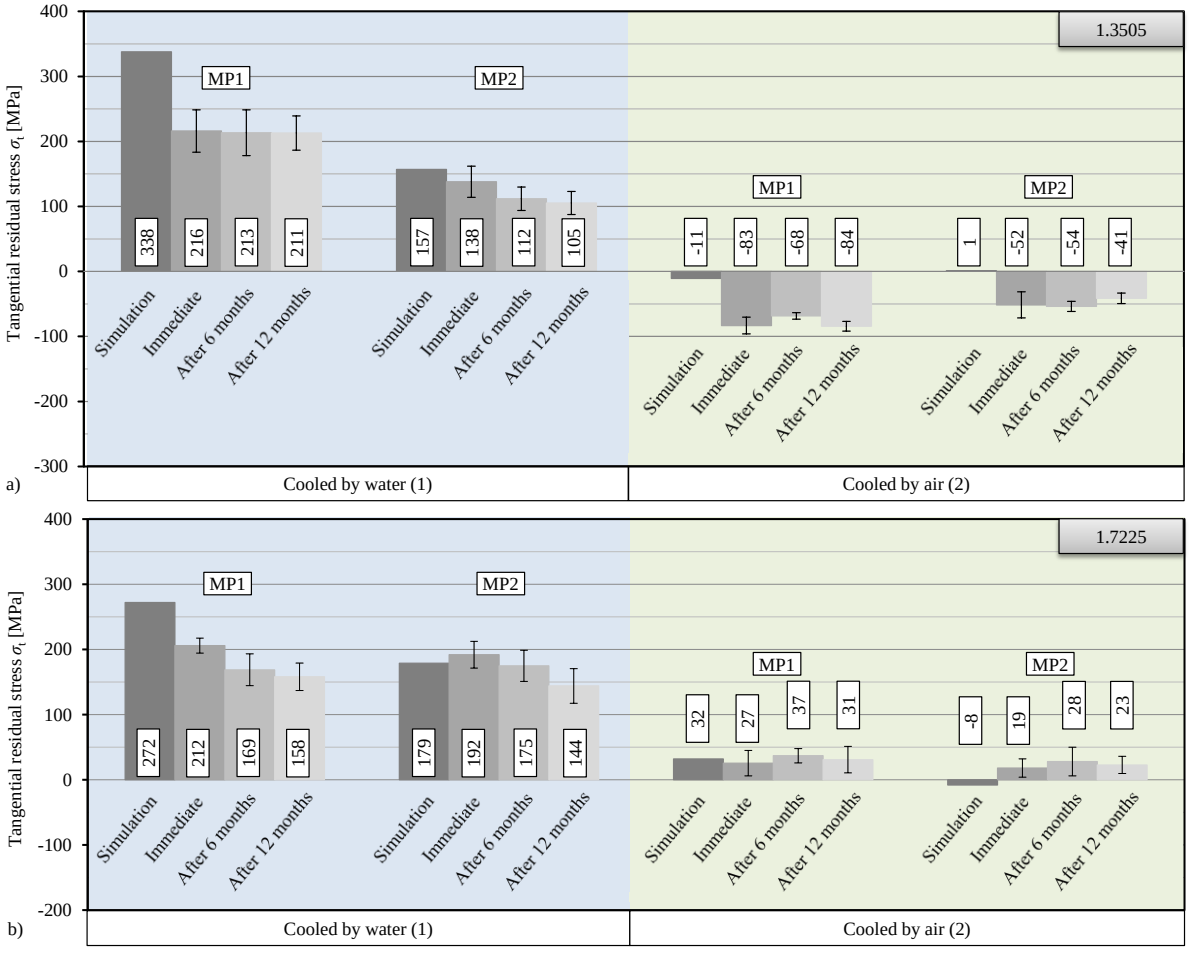

Figure 7: Calculated tangential residual stresses σ_t in comparison with the results of the experimental long-term residual stress analyses.

It is noted that cooling of the specimens in water causes positive residual stresses in both materials. Furthermore, cooling of the specimens made of 1.7225 in air lead to positive residual stresses as well. Negative residual stresses are only measured for the air-cooled specimens of material 1.3505. This is primarily due to the changed phase transformation behaviour of 1.3505 during slow cooling. At rapid cooling in water, a martensitic phase transformation occurs for both materials first in the specimen surface and afterwards in the specimen core. Each time this phase transformation is associated with volume expansion due to the larger lattice constants of the

martensitic phase compared to the austenitic phase. Since the volume expansion occurs last in the specimen core, a strain gradient is created in the material, which leads to positive stresses at the specimen surface and negative residual stresses in the specimen core. When the specimens from 1.3505 are cooled in air, the volume expansion during the transformation of the austenitic to the pearlitic phase is significantly smaller. In addition, the transformation already takes place at high temperatures between 700 °C and 600 °C (cf. Figure 3a). Following the pearlitic phase transformation, the specimen is further cooled down from about 600 °C to room temperature. Due to free convection, the specimen surface cools down faster than the specimen core. Once the surface temperature of the sample reaches room temperature, thermal shrinkage of the core continues. In contrast to the water-quenched specimens, where a volume expansion due to the martensitic transformation occurs in the end of cooling in the core, a thermal shrinkage of the core appears here. This leads to a strain gradient between the specimen surface and the specimen core, which results in negative residual stresses on the specimen surface and positive residual stresses in the core. The effect of the bainitic phase transformation in the material 1.7225 compared to the pearlitic phase transformation in the material 1.3505 starts much later in the temperature range from 400 °C to 600 °C (cf. Figure 3b). The volume expansion as a result of the bainitic phase transformation and the thermal shrinkage compensate each other so that only low positive stresses up to a maximum of 37 MPa are measured.

Furthermore, it is observed that the amount of residual stresses on the thick-walled side (MP1) of the specimen cooled by water are always higher than on the thin-walled side (MP2). According to the asymmetrical geometry of the specimen, an inhomogeneous residual stress profile is generated on the circumference of the specimen.
The residual stresses were applied reproducibly in each case with an absolute standard deviation of less than 30 MPa by the experimental setup described in section 3. Accordingly, it can be assumed that technologically reproducible residual stresses can also be generated targeted to components in further hot forming processes.
The comparison of the experimentally measured residual stresses and the values obtained from simulations shows that the developed FE-model is suitable for a good prediction accuracy of the residual stresses. In particular, the differences in the amount of residual stresses during cooling in water between the thick-walled side (MP1) and the thin-walled side (MP2) of the specimen are calculated properly in the simulations.

Repeating measurements after six months and twelve months show that the residual stresses generated, remain essentially stable in the material. In particular, at MP1 on the specimen of the material 1.3505 which were cooled in water, hardly show any changes in residual stresses with respect to time. In contrast, at the measuring points on the specimens of the material 1.7225 cooled by water, a slight decrease in the tangential residual stresses is observed over time. Despite storage at the constantly low temperature of 20 °C, stress relaxation has occurred. In contrast, the measured values of the stresses on the specimen cooled in air show generally lower initial residual stresses and barely changes in the stresses during the long-term investigations.
It should be noted that the residual stresses arising from the thermomechanical process are significantly influenced by the phase transformations. These transformations take place on the atomic level. With the X-ray method, the residual stresses on a macroscopic level can be measured exclusively. The complex interrelations between the residual stresses of the second and third type on the microscopic scale and their influence on the stability of the residual stresses of the first type on the macroscopic scale can therefore not be measured experimentally. For this reason, a working group of the authors is simultaneously engaged in modelling the effects of the microscopic processes using FE^2 simulations based on the macroscopic calculations from this work [31]. With such multiphase approaches, an improved numerically supported statement on the stability of the residual stresses should be possible in the future.
For an advanced model validation, the measurements of residual stresses on the circumference of the specimen surface at different angles θ corresponding to Figure 5c were also evaluated. Figure 8 shows a comparison of the calculated and experimentally determined residual stress values.
In addition, the contour plots for the distribution of the tangential residual stresses on the specimen surface of each case are shown in the top of Figure 8. The simulations reveals that a homogeneous distribution of the equivalent plastic strain occurs on the surface of the specimens. Equivalent plastic strain values of ε_{eq}=0.46 at MP1 and ε_{eq}=0.47 at MP2 for the material 1.3505 as well as ε_{eq}=0.52 at MP1 and ε_{eq}=0.5 at MP2 for the material 1.7225 are calculated. The comparison of results for both materials in Figure 8 shows that the residual stress profile can also be predicted with good quality over the course of the circumference. On the specimens out of 1.3505 cooled in water, a slightly decreasing stress curve can be observed from MP1 (θ = 0°) to MP2 (θ = 180°). In contrast, the stress profile of the specimens made of 1.7225 shows slight oscillations with a minimum at θ = 90° and a maximum

at θ = 135°. The residual stresses of specimens cooled in air are constantly low for both materials. In this way, the developed FE simulation model could be validated for different cooling conditions at different measuring points of the specimen with eccentric hole.

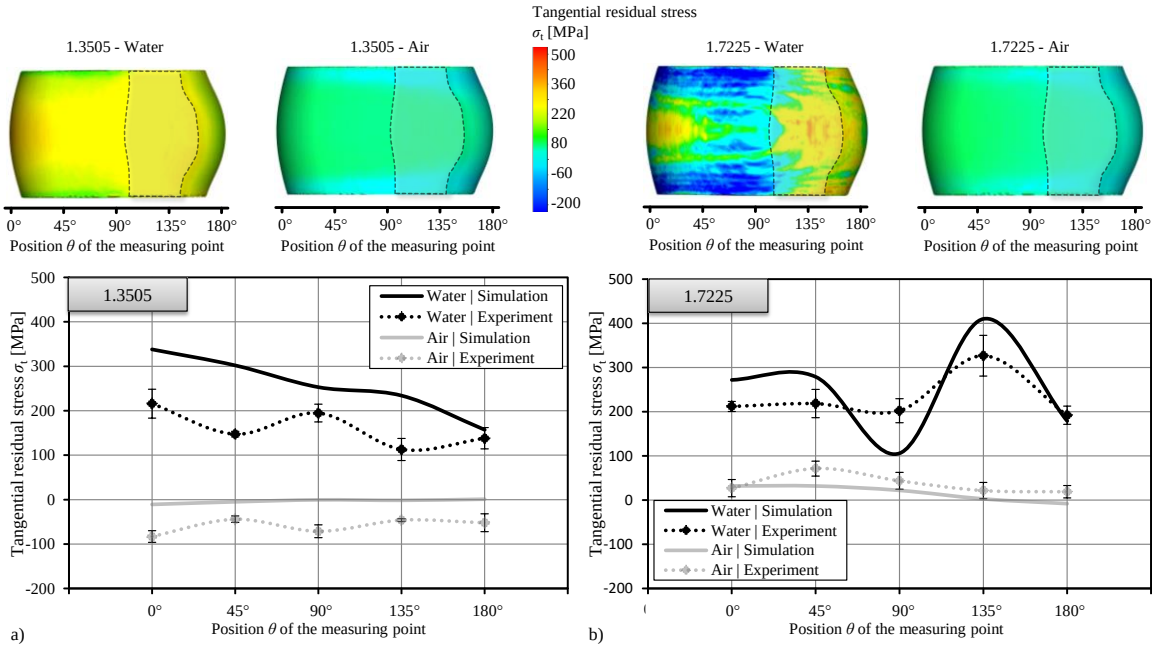

Figure 8: Contour plots of the tangential residual stress σ_t from the simulations (top) as well as comparison with experimental results on the specimens' circumferential surface (bottom) with respect to the measuring position θ for the materials 1.3505 (a) and 1.7225 (b).

5. Summary and outlook

In the scope of this work, a material model for the simulation of the interrelated thermal, metallurgical and mechanical interactions during hot forming was created with the aim of residual stress-prediction for the materials 1.3505 and 1.7225. Furthermore, a reference process of hot forming was investigated using cylindrical specimen with eccentric holes regarding the residual stresses resulting from two different cooling procedures (cooling medium water or air) by X-ray diffraction. It was found that the residual stresses can be generated by the hot forming process in a technologically replicable manner. A long-term study showed that the residual stresses are mostly stable over time, whereby slight stress relaxation was observed. Based on the extensive experimental results, the developed FE model of the hot forming process could finally be validated.

In a next step, the stability of the residual stresses resulting from the hot forming processes should be investigated under cyclic mechanical and thermal loads. Besides, the validated numerical model can be used to predict residual stresses in complex industrial processes. The overall objective of the work is the FE based process design for targeted application of residual stresses to improve the properties of hot formed components.

Acknowledgement

Funded by the German Research Foundation (DFG, Deutsche Forschungsgemeinschaft) - 374871564 (BE 1691/223-2, BR 5278/3-2, SCHR 570/33-2) within the priority program SPP 2013.

References

[1] B. Verlinden, J. Driver, J. Samajdar und R. Doherty, „Thermo-mechanical processing of metallic materials“.*Elsevier Science 11*.

[2] D. Brands, A. Chugreev, C. Kock, R. Niekamp, L. Scheunemann, S. Uebing, B.-A. Behrens und J. Schröder, „On the analysis of microstructural residual stresses in hot bulk forming parts under specific cooling“ *Proceedings in Applied Mathematics and Mechanics*, 2018.

[3] R. C. McClung, „A literature survey on the stability and significance of residual stresses during fatigue“ *Fatigue & Fracture of Engineering Materials & Structures*, Nr. 30, pp. 173-205, 2007.

[4] W. Zhuang und B. Wicks, „Mechanical surface treatment technologies for gas turbine engine components“ *Journal of Engineering for Gas Turbines and Power,* 2003.

[5] B. Eigenmann, V. Schulze und O. Vöhringer, „Surface residual stress relaxation in steels by thermal or mechanical treatment“ *Proceedings of the Fourth International Conference on Residual Stresses, Society of Experimental Mechanics,* pp. 598-607, 1994.

[6] J. T. Cammett, C. A. Sauer und T. E. Arnold, „Observations of Shot Peening Residual Stresses in 17 Cr - 7 Ni Austenitic Stainless Steel and Their Redistribution Via Mechan“ *The Fifth International Conference on Shot Peening: ICSP5,* pp. 282-289, 1993.

[7] A. Wick, V. Schulze und O. Vöhringer, „Effects of warm peening on fatigue life and relaxation behaviour of residual stresses in AISI 4140 steel“ *Materials Science and Engineering: A,* pp. 191-197, 2000.

[8] K. Iida und Y. Hirose, „The residual stress distribution in shot peened carburized steel under fatigue“ *Proceedings of the 7th International Conference on Shot Peening,* pp. 96-101, 1999.

[9] D. A. Clark und W. S. Johnson, „Temperature effects on fatigue performance of cold expanded holes in 7050-T7451 aluminum alloy“ *International Journal of Fatigue,* pp. 159-165, 2003.

[10] B.-A. Behrens, A. Bouguecha, M. Vucetic und A. Chugreev, „Advanced Wear Simulation for Bulk Metal Forming Processes“ *MATEC Web of Conferences,* 2016.

[11] B.-A. Behrens, A. Bouguecha, C. Bonk und A. Chugreev, „Experimental investigations on the transformation induced plasticity in a high tensile steel under varying thermo-mechanical loading“ *Computer Methods in Materials Science,* pp. 36-43, 2017.

[12] B.-A. Behrens und P. Olle, „Consideration of phase transformations in numerical simulation of press hardening“ *Steel Research International,* pp. 784-790, 2007.

[13] S. Denis, E. Gautier, A. Simon und G. Beck, „Stress-phase-transformation interactions - basic principles, modelling and calculation of internal stresses“ *Materials Science and Technology,* p. 805–814, 1985.

[14] W. Mitter, „Umwandlungsplastizität und ihre Berücksichtigung bei der Berechnung von Eigenspannungen“ *Materialkundlich-Technische Reihe,* 1987.

[15] B.-A. Behrens, A. Chugreeva und A. Chugreev, „FE-simulation of hot forging with an integrated heat treatment with the objective of residual stress prediction“ *AIP Conference Proceedings,* 2018.

[16] DIN EN ISO 683-17, *Heat-treated steels, alloy steels and free-cutting steels – Part 17: Ball and roller bearing steels,* Berlin: Beuth-Verlag, 2014.

[17] DIN EN 10083-3, *Steels for quenching and tempering – Part 3: Technical delivery conditions for alloy steels,* Berlin: Beuth-Verlag, 2007.

[18] B.-A. Behrens, J. Schröder, D. Brands, L. Scheunemann, R. Niekamp, A. Chugreev, M. Sarhil, S. Uebing und C. Kock, „Experimental and numerical investigations on the development of residual stresses in thermo-mechanically processed Cr-alloyed steel 1.3505“ *Metals,* Nr. 9(4), 2019.

[19] Gesellschaft für metallurgische Technologie- und Softwareentwicklung mbH, „MatILDa,“ [Online]. Available: https://www.gmt-stahl.de/en/matilda-2/. [Zugriff am 08 01 2020].

[20] B.-A. Behrens, A. Chugreev und C. Kock, „Experimental-numerical approach to efficient TTT-generation for simulation of phase transformations in thermomechanical forming processes“ *IOP Conference Series, Materials Science and Engineering,* Nr. 461, 2018.

[21] B.-A. Behrens, A. Chugreev und C. Kock, „Macroscopic FE-simulation of residual stresses in thermo-mechanically processed steels considering phase transformation effects“ *XIV International Conference on Computational Plasticity. Fundamentals and Applications,* pp. 211-222, 2019.

[22] C. Acht, M. Dalgic, F. Frerichs, H. Hunkel, A. Irretier, T. Lübben und H. Surm, „Ermittlung der Materialdaten zur Simulation des Durchhärtens von Komponenten aus 100Cr6“ *Journal of Heat Treatment and Materials,* Nr. 63, pp. 234-244, 2008.

[23] „JMatPro. Practical software for materials propertie“ Sente Software Ldt., [Online]. Available: https://www.sentesoftware.co.uk/jmatpro. [Zugriff am 08 01 2020].

[24] N. Saunders, U. Guo und X. Li, „Using JMatPro to Model Materials Properties and Behavior“ *Journal of The Minerals, Metals & Materials Society,* Nr. 55, pp. 60-65, 2003.

[25] Z. Guo, N. Saunders, J. Schillé und M. A.P., „Material properties for process simulation“ *Materials Science and Engineering: A,* Nr. 1-2, pp. 7-13, 2009.

[26] DIN EN 15305:2009-1, *Non-destructive testing - Test method for residual stress analysis by X-ray diffraction,* Berlin: Beuth Verlag, 2008.

[27] B. Eigenmann und E. Macherauch, „Röntgenographische Untersuchung von Spannungszuständen in Werkstoffen—Teil 3“ *Materialwissenschaften Und Werkstofftechnik,* Nr. 27, pp. 426-437, 1996.

[28] W. Voigt, Lehrbuch der Kristallphysik, Wiesbaden: BG Teubner, 1928.

[29] A. Reuss, „Berechnung der Fließgrenzen von Mischkristallen auf Grund der Plastizitätsbedingung für Einkristalle“ *Zeitschrift der angewandten Mathematik und Mechanik,* Nr. 9, pp. 49-58, 1929.

[30] Special Metals Co, New Hartford, New York, USA, [Online]. Available: http://www.specialmetals.com/assets/smc/540 documents/pcc-8064-sm-alloy-handbook-v04.pdf. [Zugriff am 08 01 2020].

[31] S. Uebing, L. Scheunemann, D. Brands und J. Schröder, „Numerical thermo-elasto-plastic analysis of residual stresses on different scales during cooling of hot forming parts“ *XIV International Conference on Computational Plasticity. Fundamentals and Applications,* pp. 223-234, 2019.